Magnesium acceptor in gallium nitride. II. Koopmans-tuned Heyd-Scuseria-Ernzerhof hybrid functional calculations of its dual nature and optical properties

D. O. Demchenko, I. C. Diallo, and M. A. Reshchikov
Department of Physics, Virginia Commonwealth University, Richmond, Virginia 23284, USA

(Received 30 June 2017; revised manuscript received 20 March 2018; published 17 May 2018)

The problem of magnesium acceptor in gallium nitride is that experimental photoluminescence measurements clearly reveal a shallow defect state, while most theoretical predictions favor a localized polaronic defect state. To resolve this contradiction, we calculate properties of magnesium acceptor using the Heyd-Scuseria-Ernzerhof (HSE) hybrid functional, tuned to fulfill the generalized Koopmans condition. We test Koopmans tuning of HSE for defect calculations in GaN using two contrasting test cases: a deep state of gallium vacancy and a shallow state of magnesium acceptor. The obtained parametrization of HSE allows calculations of optical properties of acceptors using neutral defect-state eigenvalues, without relying on corrections due to charged defects in periodic supercells. Optical transitions and vibrational properties of Mg_{Ga} defect are analyzed to bring the dual (shallow and deep) nature of this defect into accord with experimental photoluminescence measurements of the ultraviolet band in Mg-doped GaN samples.

DOI: 10.1103/PhysRevB.97.205205

I. INTRODUCTION

Magnesium substituting for gallium atom (Mg_{Ga}) in GaN is an acceptor impurity of the highest technological importance, since it is the only successful *p*-type dopant in GaN [1]. In the past decade there were several key theoretical developments in physics of Mg_{Ga} acceptor. Lany and Zunger proposed the concept of dual nature of acceptors in GaN and ZnO [2]. In particular, they predicted that the Mg_{Ga} acceptor in GaN exhibits two distinct states: a deep ground state with a localized hole, and a metastable shallow effective-mass-like state. While calculated 0/− thermodynamic transition levels for the localized and delocalized states were similar, 0.18 and 0.15 eV, the optical transitions via these states were substantially different, 2.93 and 3.35 eV, respectively. Other groups, employing hybrid density-functional calculations, have found that the hole bound to the Mg_{Ga} acceptor in the ground state is highly localized, with 0/− transition levels of 0.23 (optical transition at 2.7 eV) [3] and 0.38 eV [4], but did not confirm the existence of the delocalized state. Recently Sun *et al.* [5] have demonstrated that neutral Mg^0_{Ga} acceptor exhibits *three* different defect states. Two of these are localized defect-bound small polarons, characterized by a hole trapped by its self-induced lattice distortion, while the third is the anisotropically delocalized state, which is effective-mass-like in the $[11\bar{2}0]$ direction and localized in all other directions. The 0/− transition levels for all three states were found to be very similar, 0.21–0.23 eV, with one of the localized states being the hole ground state.

On the other hand, there is a consensus among experimentalists that low concentrations of Mg in GaN cause a very strong ultraviolet luminescence (UVL) band with a sharp peak at ∼3.27 eV followed by several LO phonon replicas with decreasing intensities [6–9]. Figure 1 shows photoluminescence (PL) spectra at selected temperatures from freestanding GaN lightly doped with Mg ($1.3 \times 10^{17}\ cm^{-3}$) and grown by hydride vapor-phase epitaxy (HVPE) at Kyma Technologies, Inc.

At low temperature (18 K), a very strong UVL band is observed, for which a zero phonon line (ZPL) at 3.257 eV is attributed to donor-acceptor pair (DAP)-type transitions from a shallow donor to the shallow Mg_{Ga} acceptor. With increasing temperature (50 K in Fig. 1), the DAP band intensity slightly decreases, and a very similar band emerges, with the ZPL at 3.280 eV, attributed to transitions from the conduction band to the same acceptor (*e-A* transitions). The total intensity (DAP plus *eA*) of the UVL band begins to decrease with temperature at $T > 120$ K, revealing the activation energy of 186 meV in the Arrhenius plot (the inset in Fig. 1). No defect-related bands, other than the UVL band, could be found at photon energies between 2.7 and 3.3 eV before or after the quenching of the UVL band.

These experimental results are difficult to reconcile with theoretical predictions of a localized hole ground state. It is very likely that the UVL band in undoped GaN (with quantum efficiency $\eta \sim 1\%$) [10] is caused by Mg_{Ga} acceptor. This is supported by our measurements, where only the UVL band exhibits a surge in quantum efficiency, up to 20–30%, as a result of light doping with Mg. Other recent PL measurements also suggested that for Mg doping at concentrations below $10^{19}\ cm^{-3}$ the UVL band should be assigned to the Mg_{Ga} acceptor [8]. At the same time, the blue PL band at 2.7–2.9 eV, which seemingly confirms theoretical predictions, is never observed in *lightly* Mg-doped GaN. It is observed only in some *heavily* Mg-doped samples, where it likely involves other physical processes [8,11–15]. In Part I of this paper [15] we have given a detailed experimental analysis of UVL and blue PL bands. The shape of the UVL band is typical for a weak electron-phonon coupling (the Huang-Rhys factor is about 0.5), which indicates that the hole bound to the Mg_{Ga} acceptor is weakly localized. The weak localization of the hole at the Mg_{Ga} acceptor responsible for the UVL band has also been supported by optically detected magnetic resonance studies of high-purity GaN:Mg [16].

 ©2018 American Physical Society

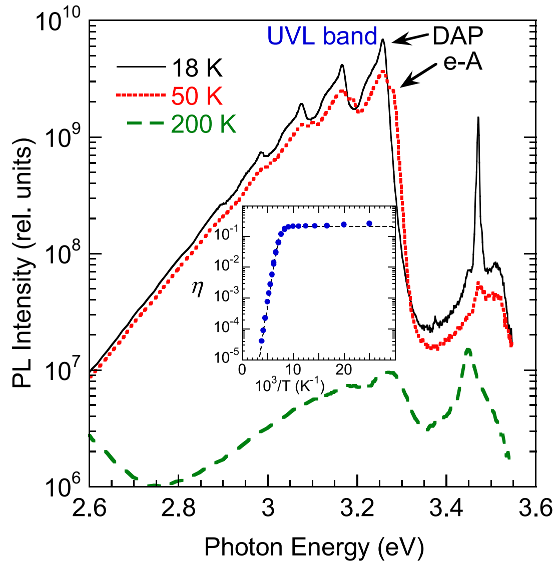

FIG. 1. PL spectra from freestanding GaN:Mg grown by HVPE method. The UVL band at $T = 18$ K includes the ZPL at 3.257 eV (attributed to DAP-type transitions involving a shallow donor and the shallow Mg_{Ga} acceptor) and a set of LO phonon replicas at distances multiple of 91 meV from the main peak. At 50 K, a series of (e-A)-type transitions appears, which corresponds to electron transitions from the conduction band to the same shallow acceptor. The inset shows the temperature dependence of the PL quantum efficiency η for the UVL band.

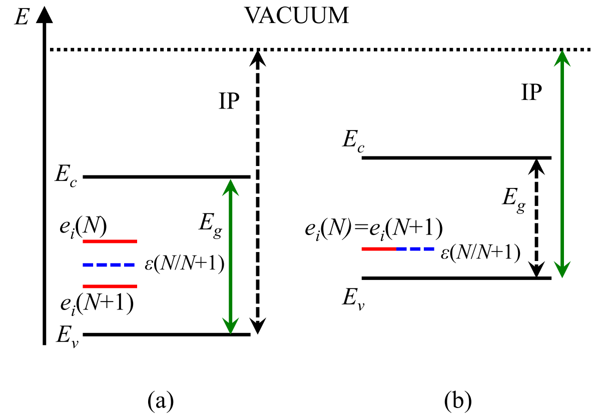

FIG. 2. Two different approaches to tuning exchange interactions in a hybrid functional: (a) fitting the band gap (solid green arrow) leads to a shift of the defect-state eigenvalue e_i with addition of an electron, and deeper transition levels; (b) fitting generalized Koopmans condition leads to the correct defect-state eigenvalues and $\varepsilon(N/N+1)$ transition level at the price of a slightly underestimated band gap (dashed arrow).

II. GENERALIZED KOOPMANS CONDITION

To resolve the above-discussed discrepancy between the experiment and theory, we calculate optical properties of defects using the Heyd-Scuseria-Ernzerhof (HSE) [17] hybrid functional, tuned to fulfill the generalized Koopmans condition [18]. The generalized Koopmans condition for defect calculations was proposed by Lany and Zunger [19–21], as a remedy for the nonlinearity of the total energy $E(N)$ with electron occupation in semi/local approximations to the density-functional theory. The main idea was to introduce a potential operator, acting on empty hole states of the host material, which would lead to the cancellation of the self-interaction energy by the wave-function relaxation upon the addition (removal) of an electron. Thus, correct eigenvalues of defect states in different charge states can be expected, leading to correct transition levels.

In contrast, hybrid functional calculations of defects in semiconductors usually resort to tuning the fraction of exact exchange in HSE in order to match the calculated band gap to the experimental value [22]. In most cases this practice works reasonably well [23,24]. However, as we show below, in such tuned HSE the correct band gap comes at a price of an excess of Fock exchange energy. As a consequence, the defect levels with respect to the valence-band maximum (VBM) are overestimated. This could be due to the valence band being pushed too far downward, potentially overestimating bulk ionization potential (IP). This is schematically shown in Fig. 2(a). For band-gap-tuned HSE, defect-state eigenvalues are not equal to defect transition levels. The defect-state eigenvalue e_i shifts downward with occupation due to the nonlinear (concave) shape of the total energy $E(N)$. The $\varepsilon(N/N+1)$ defect transition level can be found from the integration of Janak's theorem [25], i.e., the trapezoid rule places the $\varepsilon(N/N+1)$ defect transition level at an average between the unoccupied $e_i(N)$ and occupied $e_i(N+1)$ defect eigenvalues [Fig. 2(a)] [26]. This is equivalent to calculating a defect transition level as a formation energy difference of two charge states of defect. However, since in this case $e_i(N)$ is higher than $e_i(N+1)$, the self-interaction energy is overcompensated by the orbital relaxation (similarly, but to a lesser extent, to the Hartree-Fock method) [19], leading to an overestimated transition level.

In addition, in a calculation with periodic boundary conditions, a charged defect eigenvalue is also pushed downward due to the artificial electrostatic interactions in charged supercells. As a result, in practice for a relatively shallow Mg_{Ga} acceptor, the $e_i(N+1)$ in the 1− charge state is pushed below the VBM, and the 0/− transition level is effectively found between unoccupied defect eigenvalue $e_i(N)$ of neutral Mg_{Ga} and the VBM, which is an additional source of error.

The computational approach can be improved if, instead of tuning the HSE functional to reproduce the correct band gap, the generalized Koopmans condition is enforced, i.e., the HSE functional is tuned to reproduce the linear behavior of total energy with respect to occupation [Fig. 2(b)]. Since the total energy derivative with respect to occupation is equal to the eigenvalue, the transition level $\varepsilon(N/N+1)$ is equal to the defect-state eigenvalue $e_i(N)$, and $e_i(N+1)$ after correcting for the artificial electrostatic shift [Fig. 2(b)]. This tuning of HSE to correct behavior of defect eigenvalues and transition levels results in an underestimated band gap of the host. In our case this HSE tuning leads to the computed gap of GaN that is 0.27 eV below the experimental value. This could become an issue for defect levels close to the conduction band. However, since our focus is on an acceptor defect, only the energies of defect levels with respect to VBM are essential. When applying this tuning procedure to defect calculations, it is crucial to eliminate

the artificial interactions between defects in supercells. This is described in detail in Sec. IV.

III. METHODS OF CALCULATIONS

In order to tune the HSE functional to the generalized Koopmans condition for defect calculations in GaN, we have performed a series of HSE calculations of defects in GaN in supercells ranging from 72 to 300 atoms. We seek a parametrization of HSE, such that $e_i(N) = \varepsilon(N/N+1)$ in the limit of an infinitely large supercell. All calculations were performed using VASP code [27]. Both band gap and IP of a semiconductor change linearly in HSE with varying either fraction of exact exchange α or the exact exchange range-separation parameter μ. The defect-state eigenvalues and transition levels behave similarly; therefore, HSE could be tuned by varying either parameter. In literature most authors choose to vary α, while leaving μ at a typical $0.2\,\text{Å}^{-1}$. However, it has been argued that in a hybrid functional with a fraction of exact exchange equal to $1/n$, the optimal integer is $n = 4$ [28]; therefore, here we chose to keep α fixed at the standard 0.25 value, and vary the range-separation parameter μ instead. Bulk lattice constants were relaxed for each value of μ, reducing forces to less than 0.01 eV/Å. We analyzed the supercell-size scaling of unoccupied defect eigenvalues $e_i(N)$ and defect transition levels $\varepsilon(N/N+1)$. The latter is defined as $\varepsilon(N/N+1) = [E(N+1) - E(N) + \Delta]$, where $E(N+1)$ and $E(N)$ are the total energies in two different charge states and Δ is the correction for the artificial electrostatic interactions in charged supercells. The corrections were applied to the defect energies following the Lany-Zunger (LZ) procedure [29,30] throughout this paper. We also tested Freysoldt, Neugebauer, and Van de Walle correction approach [31,32], and found both methods to yield similar results. Throughout this paper, transition energies and eigenvalues are calculated with respect to the VBM of the bulk GaN. Note that in a supercell with a neutral defect the VBM is placed at $e_{\text{VBM}} + \Delta V_{0/b}$, where e_{VBM} is the bulk VBM and $\Delta V_{0/b}$ is the alignment of the averaged electrostatic potential of the neutral defect with respect to the bulk. This potential alignment is required for application of the LZ correction scheme, and was also applied to the neutral defect eigenvalues in the supercells of different sizes.

After performing calculations for a range of values of parameter μ, we conclude that HSE with exact exchange fraction $\alpha = 0.25$ and range separation parameter $\mu = 0.161\,\text{Å}^{-1}$ fulfills the generalized Koopmans condition for defects in GaN, which is demonstrated in Sec. IV.

Once the Koopmans compliant parametrization of HSE is obtained, unoccupied defect-state eigenvalue of a neutral acceptor can be used to calculate vertical optical transition energies (PL maxima) without relying on charged defect supercell corrections. Here optical properties of Mg_{Ga} acceptor in GaN were calculated with HSE ($\alpha = 0.25$, $\mu = 0.161\,\text{Å}^{-1}$) using neutral defect eigenvalues with respect to the VBM. We used the experimental value of the GaN band gap (3.50 eV) to calculate vertical optical transitions (PL maxima) between the conduction band and the defect level. Adiabatic transition levels, i.e., ZPLs, are computed by adding the 1− charge-state relaxation energies to the PL maxima, as in Refs. [33–35]. This relaxation energy is the Franck-Condon shift, i.e., the relaxation of the lattice, which defect undergoes following the radiative transition with the energy of PL maximum. Thus, in the relaxation energy calculation the errors due to artificial electrostatic interactions cancel out.

In order to construct the configuration coordinate (CC) diagram, we use harmonic approximation, fitting parabolas into the calculated optical transitions and ZPLs. This is essentially mapping the multidimensional potential-energy surface of the defect onto a one-dimensional single effective vibrational mode, which is done along the line that linearly interpolates between the equilibrium geometries of the ground- and excited-state lattices. This effective vibrational mode corresponds to the displacement of all atoms in the unit cell between the two energy minima. We tested the validity of the harmonic approximation by direct HSE calculations, using the nudged elastic band method (NEB). The two relaxed lattices of two localized polarons are set up as the first and last fixed images in the NEB calculation. Three equidistant lattice geometries were created by linearly interpolating atomic coordinates between the two equilibrium lattices. Then, as typical in a NEB calculation, the structures were allowed to relax in the directions perpendicular to the normal between the images, keeping the distance between images constant. Upon relaxation, we obtain the curvatures of parabolas of the localized polaronic states, as well as the barriers between them. All calculations were performed in 300-atom hexagonal supercells at the Γ point, with plane-wave energy cutoffs of 500 eV. All atoms were relaxed with HSE to minimize forces to 0.05 eV/Å or less (total energies of relaxed structures are converged to ∼2 meV).

Once the complete CC diagram is obtained, we numerically solve one-dimensional vibrational problem in the CC potential to obtain vibrational energies and wave functions. This is done in two steps. First, a textbook vibrational problem for the ground-state potential, i.e., 1− charge-state parabola, helps us obtain a mass-to-spring constant ratio for this effective vibrational mode. In this case, vibrational energies are known from the measured phonon replicas (Fig. 1). Second, we use this mass-to-spring constant ratio to numerically solve the vibrational problem in the excited state, i.e., the triple-well CC potential of the neutral acceptor (two small polarons and anisotropically delocalized state, Sec. V). The resulting vibrational energies and vibrational wave functions are used to analyze the optical properties of Mg_{Ga}.

The validity of the one-dimensional CC diagram model for vibrational problem in applications to the defect luminescence in semiconductors has been extensively described in Refs. [36,37]. An excellent brief analysis of its applicability and limitations is given in the appendix to Ref. [38], where it is shown that such CC diagram provides an excellent approximation for the defects that exhibit strong electron-phonon coupling (Huang-Rhys factor $S \gg 1$), which is the case for strongly localized polaronic states of Mg_{Ga}. Also, for the defects with weak electron-phonon coupling (Huang-Rhys factor $S < 1$), the model reproduces overall PL line shape correctly, although it cannot exactly reproduce the fine structure of the PL bands, e.g., for $S = 0.3$, the phonon replicas of the PL could be shifted by 0.02–0.04 eV. Therefore, for a

weakly localized defect state of Mg acceptor, with Huang-Rhys factor $S \sim 1$, it is expected that the one-dimensional CC diagram model is accurate to within roughly 0.02–0.04 eV.

It is also useful to know if this tuning of HSE reproduces the experimental IP. However, this is difficult to assess because there is a significant scatter in experimental IP values. For example, typical photoemission measurements of IP or electron affinity yield the values of IP for GaN between 6.2 and 7.2 eV [39–46], evidently due to varying surface conditions. Therefore, we also calculated the bulk IP of GaN for a range of HSE parameters, following the approach presented by Hinuma *et al.* [47], using 36-atom GaN slabs and 20-Å layers of vacuum, with surfaces along the nonpolar $[11\bar{2}0]$ direction. Tests on 68-atom slabs with 28-Å layers of vacuum confirm the convergence of the approach.

IV. TUNING HSE HYBRID FUNCTIONAL FOR DEFECT CALCULATIONS IN GaN

A. Relaxed Mg_{Ga} acceptor

First, we analyze supercell-size scaling of eigenvalues and transition energies of relaxed lattice of Mg_{Ga} acceptor in GaN. In the case of Mg_{Ga}, the N-electron state corresponds to the neutral acceptor, and $(N+1)$ state to the 1− charge state. The shift of $e_i(N+1)$ below the VBM prevents a straightforward application of the tuning procedure, i.e., adjusting exact exchange-range separation in HSE so that $e_i(N) = e_i(N+1)$ [20]. In addition, neutral Mg_{Ga} exhibits significant delocalization errors. This is illustrated in Fig. 3, where HSE-computed ($\alpha = 0.25$ and $\mu = 0.161$ Å^{-1}) unoccupied neutral Mg_{Ga} eigenvalue $e_i(N)$ is shown along with uncorrected and corrected (using the LZ scheme) $\varepsilon(0/-)$ transition energy as functions of the inverse supercell size. Eigenvalues and transition energies are plotted with respect to the VBM of the bulk GaN.

The nonmonotonic behavior of both unoccupied defect eigenvalue $e_i(N)$ and transition energy $\varepsilon(0/-)$ illustrates two competing error sources in this case. One is the spurious electrostatic energy due to periodic supercells, which leads to an upward trend in eigenvalue and transition energy with increasing supercell size. Another is the delocalization energy due to the overlap of the defect-induced wave functions, which leads to the downward energy trend with the supercell size. Figure 3 also shows the defect-state spin density (defect-state eigenvalue of neutral acceptor is occupied in one spin only) computed in 72-, 128-, and 300-atom supercells. In all cases ionic relaxations were started from the same initial defect geometries, where the Mg-N bond length along the wurtzite c axis was increased by 0.2 Å from the ideal bulk GaN value, in order to induce the lattice relaxation self-trapping of a hole, i.e., small polaron. However, in cases of 72- and 128-atom supercells the small polaron is not fully reproduced due to significant overlap between defect-state wave functions. In these supercells the wave functions overlap dominates the energy error, leading to the downward trend of transition energy and defect eigenvalue. In contrast, in a 300-atom supercell a well-localized polaronic defect state is obtained, and the energy error is mostly electrostatic. Therefore, it is difficult to reliably establish size scaling of the localized polaronic states of Mg_{Ga}, and to check the Koopmans compliance of HSE for polaronic states. It is necessary to separate the delocalization and the electrostatic errors in order to obtain converged values of $e_i(N)$ and $\varepsilon(0/-)$ in the limit of an infinitely large supercell.

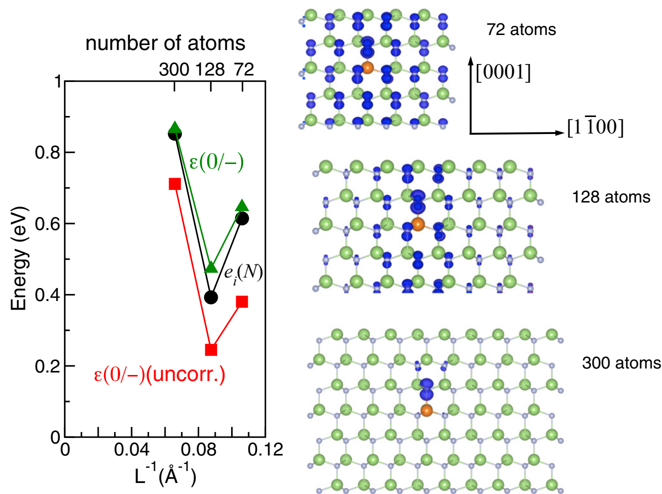

FIG. 3. Unoccupied neutral defect eigenvalue $e_i(N)$ (black circles), uncorrected (red squares), and corrected (green triangles) $\varepsilon(0/-)$ transition energies as functions of the inverse supercell size for a relaxed lattice geometry of Mg_{Ga} acceptor. Energies are plotted with respect to the bulk GaN VBM. The isosurfaces of the defect-state spin density of neutral Mg_{Ga} are plotted at 5% of their maximum values for three supercell sizes. Large orange atom is Mg, large green atoms are Ga, and small gray atoms are N.

B. Unrelaxed Mg_{Ga} acceptor

To eliminate polaronic effects during HSE tuning, we fix the atomic positions at those of the bulk GaN and perform calculations for unrelaxed Mg_{Ga} defect geometries. The resulting scaling of $e_i(N)$ and $\varepsilon(0/-)$ is shown in Fig. 4.

The downward trend of the defect eigenvalue and transition energy [Fig. 4(a)] with supercell size is indicative of the dominating contribution from the delocalization energy (i.e., defect wave-function overlap). The dashed lines in Fig. 4(a) are fits of $aL^{-1} + bL^{-3} + c$ to HSE-computed transition energies, showing the expected energy scaling if the errors were dominated by the electrostatic interactions. The extrapolations of corrected and uncorrected transition energies are widely different, suggesting that standard electrostatic error corrections are not appropriate in this case. The reason for this is revealed in average electrostatic potentials computed in 300-atom supercell for neutral and 1− charge states of Mg_{Ga}, shown in Fig. 4(b). The neutral Mg_{Ga} defect electrostatic potential is not approaching a constant value between defects, indicating electrostatic interaction between neutral Mg acceptors. In addition, the LZ electrostatic error correction scheme includes an alignment of the neutral defect potential to that of the bulk. However, the neutral defect potential is unconverged with respect to supercell size. This, along with interacting neutral defects, leads to the inconsistent scaling of the corrected and uncorrected 0/− transition energies.

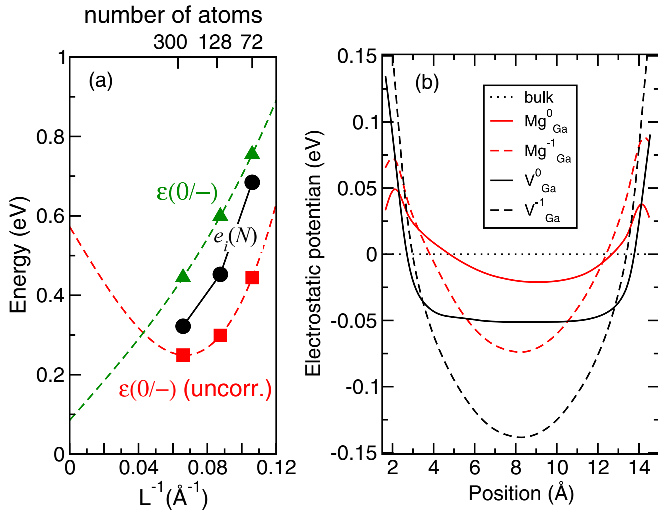

FIG. 4. (a) Unoccupied neutral defect eigenvalue $e_i(N)$ (black circles), uncorrected (red squares), and corrected (green triangles) $\varepsilon(0/-)$ transition energies as functions of the inverse supercell size for an unrelaxed lattice geometry of Mg_{Ga} acceptor. Energies are plotted with respect to the bulk GaN VBM. Dashed lines are extrapolations of electrostatic interactions to the limit of infinite supercells. (b) Average electrostatic potential for neutral and 1− charge states of Mg_{Ga} and gallium vacancy V_{Ga} along $\mathbf{a}_1$ vector of the 300-atom supercell. The potential is averaged over transversal planes and along $\mathbf{a}_1$ with a periodicity of GaN lattice constant. The defect is at the origin with its periodic image at 16.06 Å.

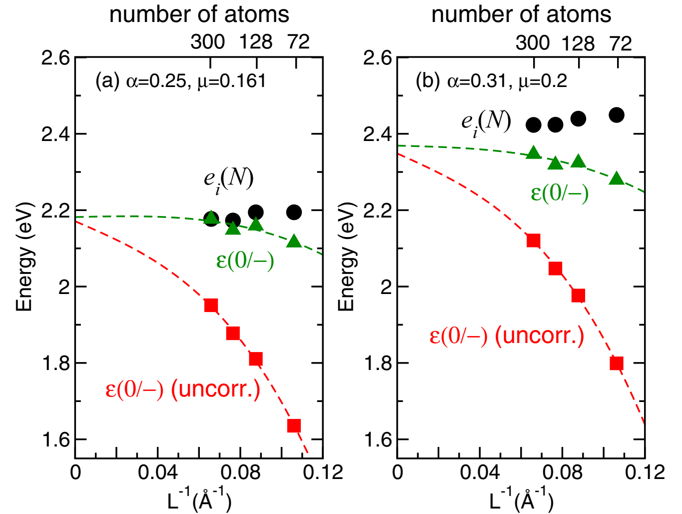

FIG. 5. Unoccupied neutral defect eigenvalue $e_i(N)$ (black circles), uncorrected (red squares), and corrected (green triangles) $\varepsilon(0/-)$ transition energies as functions of the inverse supercell size for the unrelaxed lattice geometry of gallium vacancy V_{Ga}. Results obtained by two parametrizations of HSE hybrid functional, $\alpha = 0.25$, $\mu = 0.161$ Å^{-1} (a), fitted to fulfill the generalized Koopmans condition; and $\alpha = 0.31$, $\mu = 0.2$ Å^{-1} (b), fitted to reproduce experimental band gap. Energies are plotted with respect to the bulk GaN VBM. Dashed lines are extrapolations of electrostatic interactions to the limit of infinite supercells.

Although the spurious electrostatic interactions of neutral defects are not as significant as those of negatively charged Mg_{Ga}, they are sizable and therefore partially cancel out in the calculation of 0/− transition energy. Furthermore, for negatively charged acceptors electron delocalization leads to partial screening of interactions of charged Mg_{Ga} defects. This is shown in Fig. 4(b) by comparing averaged electrostatic potential of Mg_{Ga} with that of a "well-behaved" deep-level defect, such as gallium vacancy V_{Ga}. First, the averaged potential between neutral vacancies is constant, indicating no electrostatic interactions. Second, comparison of averaged potentials of negative Mg_{Ga} and V_{Ga} defects shows that negatively charged Mg acceptors interact weakly in comparison with vacancies. Since transition energies of V_{Ga} scale predictably, and are well corrected by the LZ error correction scheme (as shown in Sec. IV C.), the weak interaction of negative Mg_{Ga} defects suggests that this procedure will result in overcorrection in the latter case. Thus, there are three problems with fitting a HSE functional to generalized Koopmans condition for Mg acceptor: significant delocalization of defect states, electrostatic interactions between neutral defects, and weaker than expected electrostatic interaction between charged defects. The latter two partially cancel each other, leading to the delocalization error being dominant in the scaling of transition energy and defect eigenvalue with supercell size. All this suggests that a better choice for fitting the HSE hybrid functional for defect calculations would be a defect that does not exhibit these complications, such as gallium vacancy [Fig. 4(b)].

C. Unrelaxed gallium vacancy V_{Ga}: A deep defect state

Figure 5 shows supercell-size scaling of the defect-state eigenvalue and corresponding transition level of unrelaxed gallium vacancy V_{Ga} obtained using two parametrizations of HSE hybrid functional, $\alpha = 0.25$, $\mu = 0.161$ Å^{-1} [Fig. 5(a)], which fulfills the generalized Koopmans condition, and commonly used $\alpha = 0.31$, $\mu = 0.2$ Å^{-1} [Fig. 5(b)], which reproduces the experimental value of the band gap. The unoccupied defect-state eigenvalues of neutral defects with respect to the bulk VBM (Sec. III) are nearly constant for all supercell sizes. Since the electrostatic potential of the neutral gallium vacancy is well converged far from the defect [Fig. 4(b)], both uncorrected and corrected $\varepsilon(0/-)$ transition energies, shown in Fig. 5, exhibit expected scaling due to artificial electrostatic interactions of charged defects, both extrapolating to the same value at the infinitely large supercell limit. The LZ correction scheme effectively eliminates the artificial electrostatic energy in supercells of 128 atoms and larger. The HSE hybrid functional parametrization obtained in this work, $\alpha = 0.25$, $\mu = 0.161$ Å^{-1}, enforces the generalized Koopmans condition [Fig. 5(a)]. The neutral (unoccupied) defect-state eigenvalue $e_i(N)$ and transition energy $\varepsilon(0/-)$ are practically equal to each other in a 300-atom supercell. The extrapolation of corrected transition energy shows a nearly constant value up to an infinitely large supercell. On the other hand, a commonly used parametrization of HSE, $\alpha = 0.31$, $\mu = 0.2$ [Fig. 5(b)], which reproduces the correct band gap, does not fulfill the Koopmans condition. Although the difference between defect-state eigenvalue $e_i(N)$ and transition energy

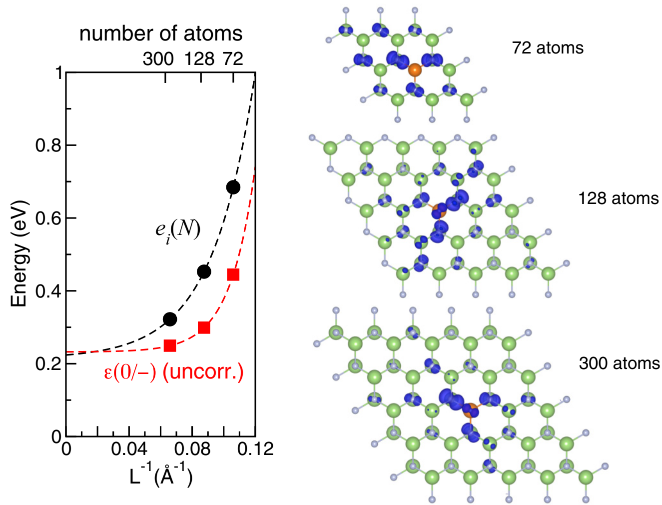

FIG. 6. Unoccupied neutral defect eigenvalue $e_i(N)$ (black circles) and uncorrected $\varepsilon(0/-)$ transition energies (red squares) as functions of the inverse supercell size for an unrelaxed lattice geometry of Mg_{Ga} acceptor. Energies are plotted with respect to the bulk GaN VBM. Dashed lines are exponential fits, extrapolating to the limit of infinite supercells. The isosurfaces of the defect-state spin density are plotted at 5% of their maximum values for three supercell sizes. Large orange atom is Mg, large green atoms are Ga, and small gray atoms are N. The view is along the [0001] direction.

$\varepsilon(0/-)$ is rather small, about 0.1 eV, both values are shifted upward in the band gap by about 0.2 eV. This makes defect states and transition levels too deep, indicating an excess of exact exchange energy in the HSE functional, which also tends to overlocalize the wave functions. As previously shown in Ref. [22], increasing the amount of exact exchange in a hybrid functional leads to the valence band shifted linearly downward, while the deep defect level (such as that of V_{Ga}) stays practically fixed with respect to some physical reference, such as average electrostatic potential, a core electron level, or vacuum. Therefore, the difference in transition levels of V_{Ga} in Figs. 5(a) and 5(b) originates mostly from the VBM shifting downward with increased amount of exact exchange. Thus, the Koopmans-compliant HSE parametrization [Fig. 5(a)] is a better choice for defect calculations, in spite of yielding a somewhat underestimated band gap. The trade-off is the correct defect eigenvalues and transition levels with respect to the VBM and self-interaction free defect-state wave functions.

D. Unrelaxed Mg_{Ga} acceptor: A weakly localized defect state

Up to this point, we have shown that the above HSE is tuned to the generalized Koopmans condition for 0/− transition level of one defect, gallium vacancy. Next, we test this for Mg_{Ga} acceptor, which, as shown above, in unrelaxed defect lattice is a contrasting case to that of V_{Ga}. Figure 6 shows supercell-size scaling of neutral defect-state eigenvalue and corresponding transition level of unrelaxed Mg_{Ga} acceptor along with the defect-state spin densities in three different supercells. The defect-state wave functions are practically delocalized in 72-atom supercells, and weakly localized in 128- and 300-atom supercells. The electrostatic corrections are not applied in this case, since, as shown above, Mg_{Ga} acceptor does not exhibit expected electrostatic interactions in either neutral or 1− charge state, and standard corrections lead to an improper scaling of transition energies. Due to a significant delocalization in this case, the artificial interactions between the defects are dominated by the wave function overlap, as indicated by the downward scaling trend. These interactions scale exponentially with the supercell size [30,48], which is shown with dashed lines in Fig. 6. The extrapolations of unoccupied $e_i(N)$ and $\varepsilon(0/-)$ to infinite supercells are very close. It should be noted that these extrapolations are not as accurate as those for V_{Ga}. In the case of Mg_{Ga} they contain contributions from both electrostatic and delocalization errors. However, if we do not resort to extrapolations, in 300-atom supercells the difference between $e_i(N)$ and uncorrected $\varepsilon(0/-)$ is only ~0.07 eV (Fig. 6), compared to 0.23 eV for the localized state [Fig. 5(a)]. There are two reasons for this. First is the above-mentioned partial cancellation of electrostatic interaction errors of neutral and charged defects in $\varepsilon(0/-)$. Second is a significantly reduced self-interaction for a weakly localized state. In the limit of completely delocalized Bloch states, self-interaction energy is approaching zero and the Koopmans condition is always fulfilled. It would even formally be fulfilled in a semi/local approximation to the density-functional theory, even though in this case Mg_{Ga} defect state cannot be reproduced since it merges with the VBM. Similarly, a standard parametrization of HSE ($\alpha = 0.25$ and $\mu = 0.2$ Å^{-1}) is also unable to reproduce Mg_{Ga} defect state. On the other hand, a commonly used band-gap-tuned HSE with $\alpha = 0.31$ and $\mu = 0.2$ Å^{-1} yields Mg_{Ga} scaling similar to that shown in Fig. 6, with transition level close to the eigenvalue, albeit both slightly deeper in the gap. In other words, for a weakly localized defect state, such as that of unrelaxed Mg_{Ga}, the Koopmans condition is approximately fulfilled for a range of HSE parameters. Provided that these defect states are resolved, with varying α or μ in HSE these states roughly follow the shifting VBM, and acceptor ionization energy is not very sensitive to the choice of HSE parameters [24].

Thus, the HSE hybrid functional with $\alpha = 0.25$ and $\mu = 0.161$ Å^{-1} enforces the generalized Koopmans condition for a well-localized defect state, such as that of V_{Ga}, and to a good degree represents weakly localized defect states, such as that of unrelaxed Mg_{Ga} acceptor. By using this parametrization of HSE we should be able to analyze the interplay between small polarons and weakly localized state of Mg acceptor in order to correctly interpret the experimental data.

E. Relaxed Mg_{Ga} acceptor: Influence of HSE tuning on optical properties

As mentioned above, it has been shown [5] that neutral Mg_{Ga} acceptor exhibits three defect states with different wave functions. Two of them are strongly localized small polarons, and the third one is anisotropically delocalized defect state. Only the shallow acceptor state is observed in experiments, the explanation for which is presented in Sec. V B. The calculated polaronic defect states are expected to produce optical transitions with PL maxima and ZPLs separated by large (0.4–0.6 eV) relaxation energies for any set of HSE parameters.

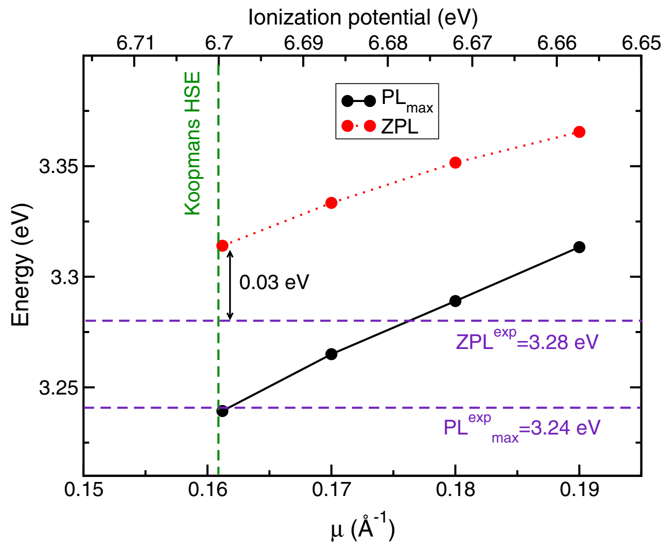

FIG. 7. Dependence of calculated optical properties of the shallow defect state of Mg_{Ga} acceptor on the range-separation parameter μ in HSE hybrid functional with $\alpha = 0.25$. Horizontal dashed lines are experimentally measured values of PL maximum (defined as a maximum of the PL band envelope) and ZPL of the UVL band shown in Fig. 1. Vertical dashed line marks a value of μ for which the generalized Koopmans condition is fulfilled. Upper horizontal axis shows IP calculated with corresponding values of μ.

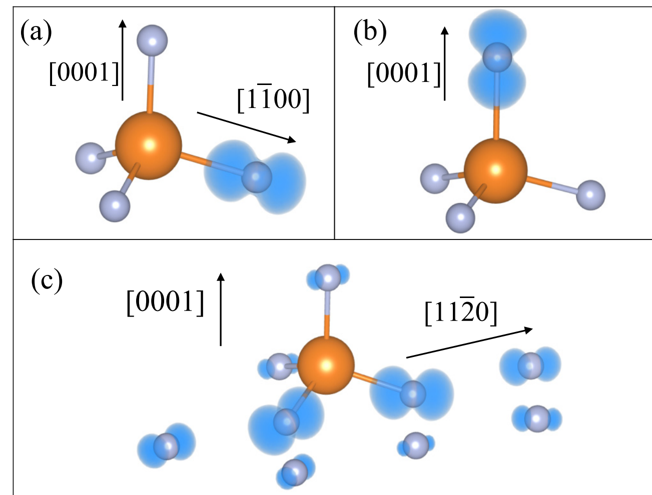

FIG. 8. Spin-density isosurfaces at 10% of maximum value of the three stable defect states of neutral Mg_{Ga} acceptor. For clarity, only nitrogen atoms around the Mg impurity are shown, and the rest of GaN host atoms are removed. Wurtzite crystallographic axes are shown to illustrate orientation of the defect states: (a) and (b) are localized small polarons and (c) is the anisotropically delocalized acceptor state.

These predicted broad defect PL bands, indicative of deep defect states, are not observed experimentally (see Sec. V B.). Figure 7 shows HSE tuning influence on optical properties of the anisotropically delocalized defect state (shallow acceptor state). The calculated results are compared to experimentally observed PL parameters.

The calculated IP linearly depends on the HSE range-separation parameter μ, which allows comparison of the optical transitions via Mg_{Ga} acceptor with varying μ and IP along the same axis. The shallow anisotropically delocalized defect state produces reasonable results for a range of HSE parameters μ. However, as shown in Fig. 7, excellent agreement with experiment is obtained for $\mu = 0.161\ \text{Å}^{-1}$, which is where the generalized Koopmans condition is fulfilled, and the PL maximum of shallow Mg_{Ga} acceptor state approaches an experimental value of 3.24 eV. The ZPL of the obtained PL band in this case is overestimated only slightly by 0.03 eV. It is also interesting to note that for these HSE parameters bulk GaN IP is calculated to be 6.7 eV, which happens to be an average value of available experimental results.

V. DUAL NATURE OF Mg ACCEPTOR

A. Small polarons and anisotropically delocalized state

As mentioned above, three distinct defect states of neutral Mg_{Ga} [5] with different lattice configurations of similar energies are two localized small polarons and one anisotropically delocalized shallow state. The latter is delocalized in the $[11\bar{2}0]$ direction of wurtzite GaN and localized in all other directions. The spin densities of three Mg^0_{Ga} defect states, calculated using the Koopmans-tuned HSE, are shown in Fig. 8. Lattice distortions that lead to the two small polaronic states (a) and (b), and the anisotropically delocalized acceptor state (c) are similar to those in Ref. [5]. Our calculations show that the lowest-energy defect state is the small polaron localized along the $[1\bar{1}00]$ direction [Fig. 8(a)]. The distortion that leads to self-trapping of the hole is the Mg–N bond length increased in this direction to 2.20 Å, compared to the other three Mg–N bonds of 2.01 Å. The state localized along the [0001] direction [Fig. 8(b)] is 12 meV higher in energy, with the Mg–N bond in this direction extended to 2.27 Å. Finally, the anisotropically delocalized state [Fig. 8(c)] is 31 meV above the lowest-energy state, with Mg–N bond lengths with localized spin density of 2.06 Å, only slightly larger than the other two of 2.03 Å.

For a well-localized acceptor state, i.e., small polaron, there is virtually no defect-state wave function overlap between adjacent supercells and no defect-state dispersion. However, a shallow acceptor state can lead to delocalization errors, so **k**-point sampling and supercell sizes are critical. Figure 9 shows the HSE band structure of neutral Mg_{Ga} acceptor calculated using 128- and 300-atom supercells, using the above-discussed HSE parameters. The bulk GaN band gap in this case is 3.22 eV, computed in **k**-point converged primitive unit cell. The 128-atom supercell calculation at the Γ point shows slight error in the band gap due to **k**-point sampling, yielding the band gap of 3.28 eV. This **k**-point sampling error is significantly reduced in 300-atom supercells, yielding the band gap of 3.23 eV, close to the converged bulk value.

Of the three possible defect states, Fig. 9 shows the band structure for the shallow state [Fig. 8(c)], which exhibits the largest dispersion. In a 128-atom supercell the defect wave-function overlap leads to a significant dispersion and an upward shift of the eigenvalues around the Γ point. In this case the bandwidth of the Mg^0_{Ga} impurity band in a 128-atom supercell in the Γ-M direction is 0.36 eV, while that in a 300-atom supercell is 0.18 eV. For a Γ-point-only calculation, the **k**-point sampling error in each case can be estimated by

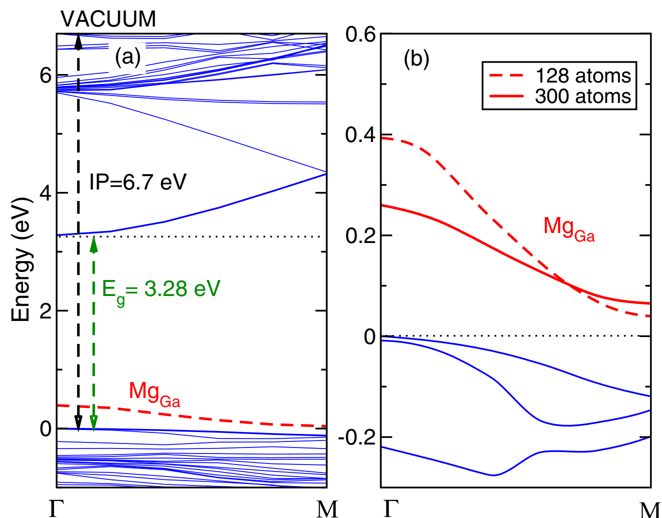

FIG. 9. Band structure of the shallow defect state of neutral Mg_{Ga} acceptor calculated using Koopmans-tuned HSE ($\alpha = 0.25$, $\mu = 0.161$ Å^{-1}). Panel (a) shows band structure obtained from 128-atom supercells. Panel (b) shows the comparison of the Mg_{Ga} impurity bands computed with 128- and 300-atom supercells, with impurity bandwidths in the Γ-*M* direction of 0.36 and 0.18 eV, respectively.

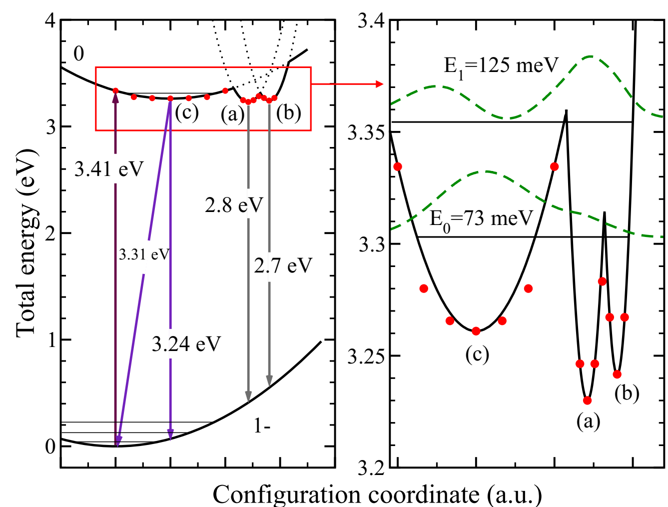

FIG. 10. Configuration coordinate diagram of Mg_{Ga} acceptor. Left panel shows full-scale CC diagram with lowest parabola corresponding to the 1− charge ground state of Mg_{Ga} acceptor. The three upper parabolas labeled (a)–(c) correspond to the three configurations of the neutral Mg_{Ga} acceptor shown in Fig. 8. Downward arrows show possible optical transitions; however, only the anisotropically delocalized acceptor state (c) is observed in experiment (see text). Right panel shows a zoomed-in configuration potential curve of the neutral Mg_{Ga} acceptor (upper parabolas in the left panel), with computed vibrational energy levels and probability densities shown with dashed lines.

finding the energy difference between the Γ-point eigenvalue and the impurity band center of mass. Since this impurity band is localized in all directions except [11$\bar{2}$0], we find this error to be −0.12 eV in a 128-atom supercell, which is about half of the energy of the defect transition level itself. For a 300-atom supercell this error is −0.05 eV. In both cases this error is partially canceled by the potential alignment of eigenvalues to the bulk VBM (Sec. IV C). However, the impurity band center of mass in a 128-atom supercell is also shifted upward by ∼0.07 eV compared to that of the 300-atom supercell, due to a larger wave-function overlap. Also, using 128-atom (or smaller) supercells with a **k**-point mesh for a shallow acceptor can lead to erroneous occupations of the impurity band at **k** points far from Γ, due to the spurious band dispersion. This can lead to wrong defect charge densities, forces, and atomic relaxations. Therefore, a safer approach, adopted in this work, is to use a relatively large 300-atom supercell at the Γ point, albeit at a significantly increased computational cost. In calculations of transition levels and optical transitions, Γ-point eigenvalues are corrected using both the potential alignment to the bulk VBM and **k**-point sampling error correction. For the eigenvalue of a neutral Mg_{Ga} in a 300-atom supercell, both corrections are small, 0.015 and −0.05 eV, respectively.

B. Why localized small polaron states of Mg_{Ga} are not observed in PL experiments

Ignoring vibrational properties of Mg_{Ga}, and taking into account typically large (microseconds) lifetimes of defect PL bands, the energies of the three defect states suggest that the lowest-energy localized small polaron [Fig. 8(a)] should be responsible for the optical properties of Mg_{Ga} acceptor. Our calculations show that this defect state would produce a PL maximum at 2.8 eV, with a ZPL at 3.23 eV, and the 0/− thermodynamic transition level at 0.27 eV. This is similar to other theoretical results obtained in Refs. [3–5]. Strongly localized nature of this small polaron leads to the predicted wide PL band, with the Franck-Condon shift of 0.43 eV, which is a signature of a deep defect state. However, this prediction clearly contradicts the experiment, where a very narrow PL band is observed (Fig. 1), which is a signature of a typical shallow defect with a weakly localized hole. Varying the HSE parameters leads to slight changes in the relative energies between the three states in Fig. 8, but the hole ground state always remains well localized, with large relaxation energies, around ∼0.4–0.5 eV.

This contradiction can be resolved with the help of a detailed CC diagram for all three neutral Mg_{Ga} acceptor states, which is shown in Fig. 10. The lowest parabola in the left panel is the 1− charge state of Mg_{Ga} acceptor, with the curvature determined from the relaxation energies computed for the 1− charge state of the defect. The left panel in Fig. 10 also shows the vibrational levels of the 1− ground state, separated by 91 meV, which are obtained from the measured phonon replicas (Fig. 1). Calculated resonant absorption and subsequent relaxation energy of the neutral defect yields the curvature of the upper parabola corresponding to the anisotropically delocalized acceptor state [Fig. 8(c)]. The calculated curvature of parabola (c) is very similar to that of the 1− ground state, suggesting similar vibrational energies of the anisotropically delocalized acceptor state (c). However, the presence of the localized polaronic states (a) and (b) introduces a perturbation to the total configuration potential of the neutral Mg_{Ga} acceptor. The curvatures of the polaronic state parabolas were obtained using HSE calculations combined with the NEB method. To

test the validity of the harmonic approximation we also used this approach for the anisotropically delocalized state (c). The resulting HSE computed total energies for Mg_{Ga}^0 are shown as red circles in Fig. 10. The parabolic fits into relaxation and transition energies in Fig. 10 are in a very good agreement with these direct HSE calculations of the CC diagram. HSE calculations yield the barrier of 53 meV between the (a) and (b) localized states. The calculated barrier between the delocalized state (c) and the localized state (a) is ~100 meV [from (c) to (a)]. Assuming the same reduced masses of the local vibrational modes for both 1− and neutral states of Mg_{Ga} acceptor allows numerical solution of a vibrational problem in the total triple-well potential of Mg_{Ga}^0 (right panel of Fig. 10). We find the vibrational ground state of the Mg_{Ga}^0 to be 73 meV above the bottom of the well (a), which is 42 meV above the delocalized state minimum (c). In the ground state, the square of the vibrational wave function, shown with a dashed line in Fig. 10, exhibits a single peak around the delocalized acceptor state (c). The PL band shape can be thought of as a projection of this vibrational probability onto the 1− ground-state configuration curve (see, for example, Fig. 14 in Ref. [9]). Therefore, in this case only the shallow acceptor state can be observed as the PL peak and ZPL in experiment. The optical transitions associated with the two small polaronic states of Mg_{Ga}^0 are significantly less probable. These states do not produce separate PL bands at 2.8 and 2.7 eV, but instead may slightly distort the low-energy tail of the UVL band. Thus, upon photoexcitation, the system captures a hole and relaxes into the vibrational ground state of neutral Mg_{Ga} acceptor, from where optical transition occurs, producing an experimentally observed UVL band, with a characteristic shallow fine structure (Franck-Condon shift of 0.07 eV), a computed maximum of 3.24 eV (Fig. 10), and ZPL of 3.31 eV. From the CC diagram we also estimate the Huang-Rhys factor for this PL band to be ~1, which is close to the experimental value of 0.5. Thus, all calculated parameters are in excellent agreement with experimentally measured data for the Mg-related UVL band.

VI. CONCLUSIONS

In conclusion, we have resolved a long-standing disagreement between optical measurements of the UVL band in GaN and theoretical predictions of the strongly localized polaronic hole ground state of Mg_{Ga} acceptor. We have used the HSE hybrid functional tuned to fulfill the generalized Koopmans condition, rather than a commonly used tuning of HSE to the experimental band gap. The advantage of this approach is that it correctly reproduces the defect-state eigenvalues with respect to the VBM. In the case of acceptors, neutral defect-state eigenvalues can be used to calculate optical transition energies, without relying on corrections for the artificial electrostatic interactions in periodic supercells. The calculated results show excellent agreement with experimental PL measurements. Therefore, the HSE hybrid functional parametrization obtained in this work represents an improvement for calculations of defects in GaN, with the exception of those where the transition levels are close to the conduction band.

ACKNOWLEDGMENTS

The work was supported by the National Science Foundation (Grant No. DMR-1410125) and used the computational facilities of the VCU Center for High Performance Computing. We thank T. McMullen and M. Bishop for helpful discussions.

[1] S. Nakamura, T. Mukai, M. Senoh, and N. Iwasa, Jpn. J. Appl. Phys. **31**, L139 (1992).
[2] S. Lany and A. Zunger, Appl. Phys. Lett. **96**, 142114 (2010).
[3] J. L. Lyons, A. Janotti and C. G. Van de Walle, Phys. Rev. Lett. **108**, 156403 (2012).
[4] G. Miceli and A. Pasquarello, Phys. Rev. B **93**, 165207 (2016).
[5] Y. Y. Sun, T. A. Abtew, P. Zhang, and S. B. Zhang, Phys. Rev. B **90**, 165301 (2014).
[6] B. Monemar, P. P. Paskov, G. Pozina, C. Hemmingsson, J. P. Bergman, T. Kawashima, H. Amano, I. Akasaki, T. Paskova, S. Figge, D. Hommel, and A. Usui, Phys. Rev. Lett. **102**, 235501 (2009).
[7] M. A. Reshchikov and H. Morkoç, J. Appl. Phys. **97**, 061301 (2005).
[8] B. Monemar, P. P. Paskov, G. Pozina, C. Hemmingsson, J. P. Bergman, S. Khromov, V. N. Izyumskaya, V. Avrutin, X. Li, H. Morkoc, H. Amano, M. Iwaya, and I. Akasaki, J. Appl. Phys. **115**, 053507 (2014).
[9] M. A. Reshchikov, D. O. Demchenko, J. D. McNamara, S. Fernández-Garrido, and R. Calarco, Phys. Rev. B **90**, 035207 (2014).
[10] M. A. Reshchikov, J. D. McNamara, A. Usikov, H. Helava, and Yu. Makarov, Mater. Res. Soc. Proc. **1736**, T05 (2015).
[11] L. Eckey, V. von Gfug, J. Holst, A. Hoffmann, A. Kaschner, H. Siegle, C. Thomsen, B. Schineller, K. Heime, M. Heuken, O. Schön, and R. Beccard, J. Appl. Phys. **84**, 5828 (1998).
[12] U. Kaufmann, M. Kunzer, M. Maier, H. Obloh, A. Ramakrishnan, and B. Santic, Appl. Phys. Lett. **72**, 1326 (1998).
[13] M. A. Reshchikov, G.-C. Yi, and B. W. Wessels, Phys. Rev. B **59**, 13176 (1999).
[14] F. Shahedipour and B. W. Wessels, Appl. Phys. Lett. **76**, 3011 (2000).
[15] M. A. Reshchikov, P. Ghimire, and D. O. Demchenko, Phys. Rev. B **97**, 205204 (2018).
[16] E. R. Glaser, M. Murthy, J. A. Freitas, Jr., D. F. Storm, L. Zhou, and D. J. Smith, Physica B **401-402**, 327 (2007).
[17] J. Heyd, G. E. Scuseria, and M. Ernzerhof, J. Chem. Phys. **118**, 8207 (2003).
[18] I. Dabo, A. Ferretti, N. Poilvert, Y. Li, N. Marzari, and M. Cococcioni, Phys. Rev. B **82**, 115121 (2010).
[19] S. Lany and A. Zunger, Phys. Rev. B **80**, 085202 (2009).
[20] S. Lany, Phys. Status Solidi B **248**, 1052 (2010).
[21] S. Lany and A. Zunger, Phys. Rev. B **81**, 205209 (2010).
[22] A. Alkauskas, P. Broqvist, and A. Pasquarello, Phys. Status Solidi B **248**, 775 (2011).

[23] C. Freysoldt, B. Grabowski, T. Hickel, J. Neugebauer, G. Kresse, A. Janotti, and C. G. Van de Walle, Rev. Mod. Phys. **86**, 253 (2014).
[24] D. O. Demchenko and M. A. Reshchikov, Phys. Rev. B **88**, 115204 (2013).
[25] J. F. Janak, Phys. Rev. B **18**, 7165 (1978).
[26] P. Broqvist, A. Alkauskas, and A. Pasquarello, Phys. Rev. B **80**, 085114 (2009).
[27] G. Kresse and J. Furthmüller, Phys. Rev. B **54**, 11169 (1996).
[28] J. P. Perdew, M. Ernzerhof, and K. Burke, J. Chem. Phys. **105**, 9982 (1996).
[29] S. Lany and A. Zunger, Phys. Rev. B **78**, 235104 (2008).
[30] H.-P. Komsa, T. T. Rantala, and A. Pasquarello, Phys. Rev. B **86**, 045112 (2012).
[31] C. Freysoldt, J. Neugebauer, and C. G. Van de Walle, Phys. Rev. Lett. **102**, 016402 (2009).
[32] C. Freysoldt, J. Neugebauer, and C. G. Van de Walle, Phys. Status Solidi B **248**, 1067 (2010).
[33] P. Deák, B. Aradi, T. Frauenheim, E. Janzén, and A. Gali, Phys. Rev. B **81**, 153203 (2010).
[34] P. Rinke, A. Janotti, M. Scheffler, and C. G. Van de Walle, Phys. Rev. Lett. **102**, 026402 (2009).
[35] S. Lany and A. Zunger, Phys. Rev. B **81**, 113201 (2010).
[36] A. Alkauskas, B. B. Buckley, D. D. Awschalom, and C. G. Van de Walle, New J. Phys. **16**, 073026 (2014).
[37] A. Alkauskas, Q. Yan, and C. G. Van de Walle, Phys. Rev. B **90**, 075202 (2014).
[38] A. Alkauskas, M. D. McCluskey, and C. G. Van de Walle, J. Appl. Phys. **119**, 181101 (2016).
[39] V. M. Bermudez, J. Appl. Phys. **80**, 1190 (1996).
[40] M. Eyckeler, W. Mönch, T. U. Kampen, R. Dimitrov, O. Ambacher, and M. Stutzmann, J. Vac. Sci. Technol. B **16**, 2224 (1998).
[41] H. Kim, Z.-L. Guan, Q. Sun, A. Kahn, J. Han, and A. Nurmikko, J. Appl. Phys. **107**, 113707 (2010).
[42] T. E. Cook, Jr., C. C. Fulton, W. J. Mecouch, K. M. Tracy, R. F. Davis, E. H. Hurt, G. Lucovsky, and R. J. Nemanich, J. Appl. Phys. **93**, 3995 (2003).
[43] K. M. Tracy, W. J. Mecouch, R. F. Davis, and R. J. Nemanich, J. Appl. Phys., **94**, 3163 (2003).
[44] M. Mishra, T. C. S. Krishna, N. Aggarwal, and G. Gupta, Appl. Surf. Sci. **345**, 440 (2015).
[45] W. C. Yang, B. J. Rodriguez, M. Park, R. J. Nemanich, O. Ambacher, and V. Cimalla, J. Appl. Phys. **94**, 5720 (2003).
[46] C. I. Wu and A. Kahn, J. Appl. Phys. **86**, 3209 (1999).
[47] Y. Hinuma, A. Grüneis, G. Kresse, and F. Oba, Phys. Rev. B **90**, 155405 (2014).
[48] S. E. Taylor and F. Bruneval, Phys. Rev. B **84**, 075155 (2011).